Response of base-isolated nuclear structures to extreme earthquake shaking

Manish Kumar*†, Andrew S. Whittaker and Michael C. Constantinou

Department of Civil, Structural and Environmental Engineering; MCEER; 212 Ketter Hall, University at Buffalo, State University of New York, Buffalo, NY 14260, U.S.A.

ABSTRACT

Seismic isolation using low damping rubber and lead-rubber bearings is a viable strategy for mitigating the effects of extreme earthquake shaking on safety-related nuclear structures. The mechanical properties of these bearings are not expected to change substantially in design basis shaking. However, under shaking more intense than design basis, the properties of the lead cores in lead-rubber bearings may degrade due to heating associated with energy dissipation, some bearings in an isolation system may experience net tension, and the compression and tension stiffness may be affected by the lateral displacement of the isolation system. The effects of intra-earthquake changes in mechanical properties on the response of base-isolated nuclear power plants (NPPs) are investigated using an advanced numerical model of a lead-rubber bearing that has been verified and validated, and implemented in OpenSees.

A macro model is used for response-history analysis of base-isolated NPPs. Ground motions are selected and scaled to be consistent with response spectra for design basis and beyond design basis earthquake shaking at the site of the Diablo Canyon Nuclear Generating Station. Ten isolation systems of two periods and five characteristic strengths are analyzed. The responses obtained using simplified and advanced isolator models are compared. Strength degradation due to heating of lead cores and changes in buckling load most significantly affect the response of the base-isolated NPP.

KEY WORDS: rubber bearing, extreme loading, cavitation, nuclear power plants, isolation

1. Introduction

Low damping rubber (LDR) and lead-rubber (LR) seismic isolation bearings have been proposed for use in safety-related nuclear structures in the United States to mitigate the effects of severe horizontal earthquake shaking. The behavior of these elastomeric bearings in shear and compression is reasonably well established, and mathematical models exist to predict isolation-system responses in design basis earthquake shaking. These mathematical models use simplified load-deformation relationships (see Figure 1 for assumed shear behavior) that cannot capture behaviors that might be important for shaking more intense than design basis.

* Correspondence to: Department of Civil, Structural and Environmental Engineering, 212 Ketter Hall, University at Buffalo, State University of New York, Buffalo, NY 14260, U.S.A.
† E-mail: mkumar2@buffalo.edu

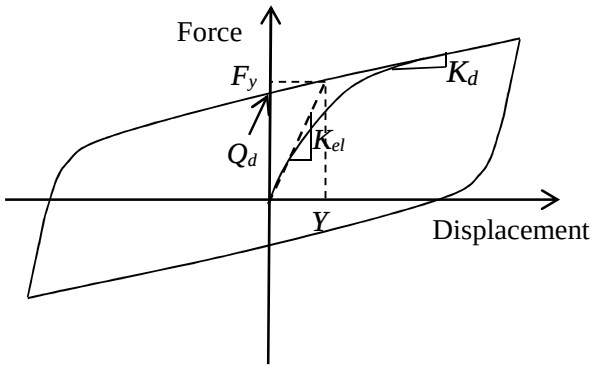

Figure 1. Simplified model of a lead-rubber bearing in shear

Models of LDR and LR bearings for analysis of safety-related nuclear structures under design basis and beyond design basis earthquake shaking should be able to accommodate the following five characteristics or behaviors:

1. Strength degradation in shear due to heating of the lead core (LR bearings)
2. Variation in buckling load due to horizontal displacement
3. Cavitation and post-cavitation behavior due to tensile loading
4. Variation in axial stiffness due to horizontal displacement
5. Variation in shear stiffness due to axial load

An advanced model that can accommodate these five characteristics has been developed by Kumar ***et al.*** (2014) and it substantially expands existing capabilities to address extreme earthquake loadings in isolated nuclear (and building) structures. The model was verified and validated following ASME best practices (ASME, 2006), and implemented in OpenSees (McKenna ***et al.***, 2006) to enable use by researchers and the design professional community. Complete details on the model are provided in Kumar ***et al.*** (2014) and only relevant information is presented in Section 2 of this paper.

A case study is performed to study the effect of these characteristics on the response of a base-isolated nuclear power plant (NPP) to extreme earthquake loadings. A two-node macro-model is created in OpenSees and subjected to thirty sets of ground motions of varying intensities generated for the site of the Diablo Canyon Nuclear Generating Station. Ten isolation systems are studied: two isolation periods and five characteristic strength ratios. The effect of each of the five characteristics on the response of the isolated structure is quantified. Results calculated using the simplified and advanced models are compared and contrasted.

2. Mathematical model of elastomeric bearings

2.1 Physical model

The physical model of an elastomeric bearing is considered as a two-node, twelve degrees-of-freedom discrete element. The two nodes are connected by six springs that represent the

mechanical behaviors in the six basic directions. The degrees of freedom and discrete spring representation of an elastomeric bearing are shown in Figure 2.

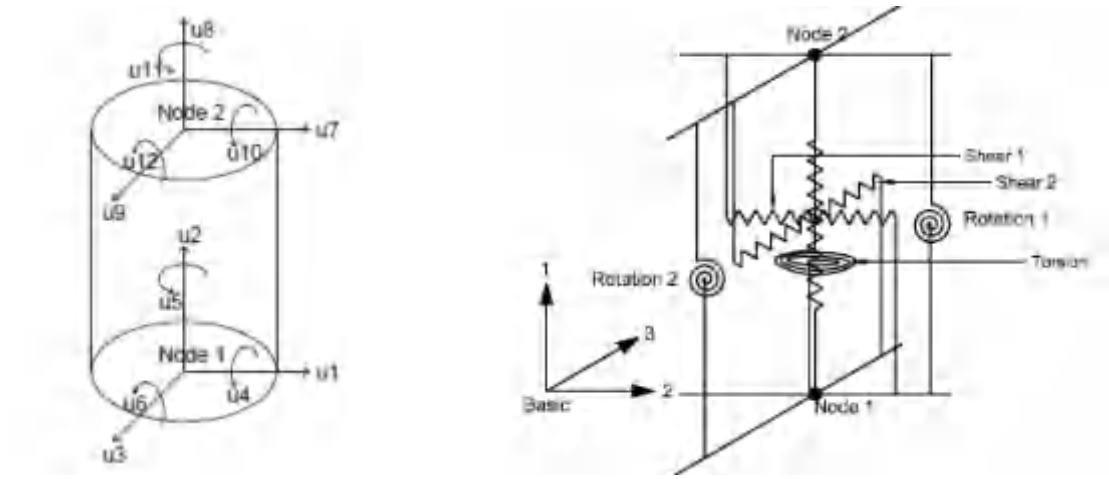

(a) Degrees of freedom (b) Discrete spring model representation

Figure 2. Physical model of an elastomeric bearing (Kumar *et al.*, 2014a)

The general form of element force vector, f_b, and element stiffness matrix, K_b, are:

$$f_b = \begin{bmatrix} Axial \\ Shear1 \\ Shear2 \\ Torsion \\ Rotation1 \\ Rotation2 \end{bmatrix}; \quad K_b = \begin{bmatrix} Axial & 0 & 0 & 0 & 0 & 0 \\ 0 & Shear1 & Shear12 & 0 & 0 & 0 \\ 0 & Shear21 & Shear2 & 0 & 0 & 0 \\ 0 & 0 & 0 & Torsion & 0 & 0 \\ 0 & 0 & 0 & 0 & Rotation1 & 0 \\ 0 & 0 & 0 & 0 & 0 & Rotation2 \end{bmatrix} \tag{1}$$

The interaction of the two shear springs is considered directly using a coupled bidirectional model. All other springs are uncoupled. The off-diagonal terms due to coupling between axial stiffness and rotational stiffnesses are ignored. The coupling of the vertical and horizontal stiffness is considered indirectly using expressions for shear and axial stiffness that depend on axial load and lateral displacement, respectively. Uncoupled linear springs are used for the three rotational springs because they do not significantly affect the response of an elastomeric bearing. The off-diagonal terms due to coupling between axial and shear, and axial and rotation, are not considered in the two-spring model (Koh and Kelly, 1987) used here. An exact model would have non-zero values of these off-diagonal terms. A discussion on the formulation of the two-spring model and the exact model is presented in Ryan *et al.* (2005). The expressions for stiffness and buckling load are derived using explicit considerations of geometric nonlinearity due to large displacements. The $P-\Delta$ effect, which is an approximate method to account for geometric nonlinearity in structural analysis problems, is therefore not considered.

2.2 Behavior under axial loading

2.2.1 Compression

The two-spring model of Koh and Kelly (1987), which was validated by Warn *et al.* (2007), is used to model the behavior of LDR and LR bearings in axial compression where the contribution of the confined lead core to compressive stiffness is ignored. The coupling of horizontal and vertical response is considered by: 1) dependence of axial stiffness on lateral displacement, and 2) variation of shear stiffness with axial load. The vertical stiffness in compression, K_v, and the horizontal stiffness, K_H, are given by (2) and (3), respectively:

$$K_v = \frac{AE_c}{T_r}\left[1+\frac{3}{\pi^2}\left(\frac{u_h}{r}\right)^2\right]^{-1} = K_{v0}\left[1+\frac{3}{\pi^2}\left(\frac{u_h}{r}\right)^2\right]^{-1} \tag{2}$$

$$K_H = \frac{GA}{T_r}\left[1-\left(\frac{P}{P_{cr}}\right)^2\right] = K_{H0}\left[1-\left(\frac{P}{P_{cr}}\right)^2\right] \tag{3}$$

where E_c is the compression modulus (Constantinou *et al.*, 2007); u_h is the horizontal displacement; r is the radius of gyration of the bonded rubber area; K_{v0} is the axial compressive stiffness at zero lateral displacement; P is the instantaneous axial load; P_{cr} is the buckling load, and K_{H0} is the horizontal stiffness at zero axial load.

The buckling load, P_{cr}, decreases with increasing horizontal displacement. The area-reduction method attributed to Buckle and Liu (1993) considers the dependence of P_{cr} on lateral displacement and provides conservative results. The model suggested by Warn *et al.* (2007) is considered here, which uses a bilinear approximation to the area-reduction method and accounts for the buckling capacity of a bearing at zero overlap area. The critical load is:

$$P_{cr} = \begin{cases} P_{cr0}\dfrac{A_r}{A} & \text{for } \dfrac{A_r}{A} \geq 0.2 \\ 0.2P_{cr0} & \dfrac{A_r}{A} < 0.2 \end{cases} \tag{4}$$

where P_{cr0} is the buckling load at zero displacement, and P_{cr} is the buckling load at overlapping area A_r of a bearing with an initial bonded rubber area of A. Figure 3 presents the mathematical model of an elastomeric bearing in compression (and tension).

2.2.2 Tension

The phenomenological model of Kumar *et al.* (2014) is used here to describe the behavior of elastomeric isolation bearings in tension. A linear force-displacement response, with axial stiffness equal to K_v, is assumed up to cavitation. The initial cavitation force in an elastomeric bearing is calculated as $F_c = 3GA$, where A is the bonded rubber area before cavitation, and the

shear modulus, G, is obtained from testing at moderate shear strains under nominal axial loads. The post-cavitation force, F, at tensile displacement u is described by the relationship:

$$F(u) = F_c\left[1+\frac{1}{kT_r}\left(1-e^{-k(u-u_c)}\right)\right] \tag{5}$$

where u_c is the initial cavitation displacement calculated by dividing F_c by K_{v0}; k is a parameter that describes the post-cavitation variation of tensile stiffness; T_r is the total rubber thickness; and other terms are defined above.

Cavitation in an elastomeric bearing is accompanied by irreversible damage due to the formation of micro cracks and cavities in the rubber volume. When a bearing is loaded beyond the point of cavitation and then unloaded, the force-displacement relationship returns along a new path and the cavitation strength is reduced. Subsequent loading follows the latest unloading path elastically until the displacement exceeds the past maximum value, $u_{\max}$, below which loading has the effect of opening and closing existing cavities only. Once the loading exceeds the past maximum value of tensile displacement, the formation of new cavities leads to increased damage, and the force-displacement relationship follows a post-cavitation behavior defined by (5). Upon load reversal, the force-displacement relationship traces a new unloading path and the cavitation strength is further reduced. The unloading paths can be approximated by straight lines between the points of maximum force and displacement $(F_{\max}, u_{\max})$ and the point of reduced force and displacement (F_{cn}, u_{cn}). Points $(F_{\max}, u_{\max})$ and (F_{cn}, u_{cn}) change with repeated cycling. To capture this behavior mathematically, a damage index ϕ is defined such that the cavitation force is given by:

$$F_{cn} = F_c(1-\phi) \tag{6}$$

and damage index ϕ is:

$$\phi = \phi_{\max}\left[1-\exp\left(-a\left(\frac{u-u_c}{u_c}\right)\right)\right] \tag{7}$$

where a defines the rate of damage, $\phi_{\max}$ is the maximum damage that can be expected in a bearing, and other terms are defined above.

Figure 3 presents the mathematical model of an elastomeric bearing in tension. The model requires the user to assign values to three parameters: k, a, and $\phi_{\max}$.

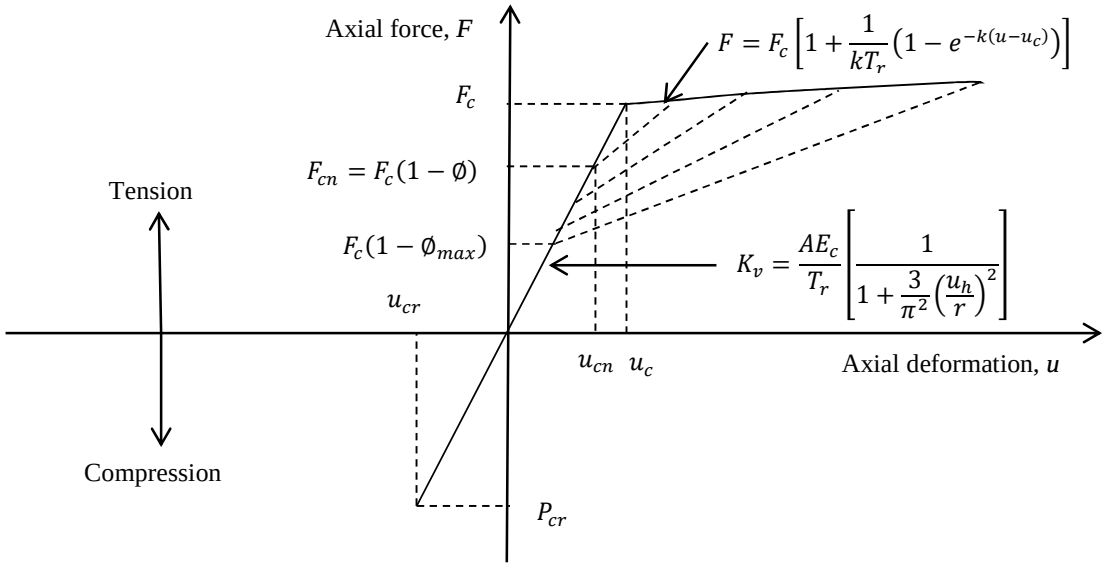

Figure 3. Mathematical model in the axial direction (Kumar ***et al.***, 2014)

2.3 Behavior under shear loading

The behavior of an elastomeric bearing in shear is well established. The Bouc-Wen model (Park ***et al.***, 1986; Wen, 1976), as extended for analysis of seismic isolation bearings and systems under bidirectional motion by Nagarajaiah ***et al.*** (1991), is used here for LDR and LR bearings. The strength degradation in a LR bearing due to heating of its lead core is addressed using the model proposed by Kalpakidis ***et al.*** (2010). The models of LDR and LR bearings in shear are discussed in Kumar ***et al.*** (2014). The model proposed by Grant ***et al.*** (2004) is implemented for high damping rubber (HDR) bearings.

2.4 Implementation and Experimental Validation

The advanced mathematical models of LDR, LR, and HDR bearings are implemented in OpenSees as three user elements: ***ElastomericX***, ***LeadRubberX*** and ***HDR*** (Kumar, 2014).

The models were validated for tensile behavior using three sets of experimental data, as shown in Figure 4. The cavitation parameter, k, and the damage index, $\phi_{\max}$, were obtained by calibration of the mathematical model with experimental data. Information on the bearings used for calibration and the values of k, a, and $\phi_{\max}$ are presented in Table 1.

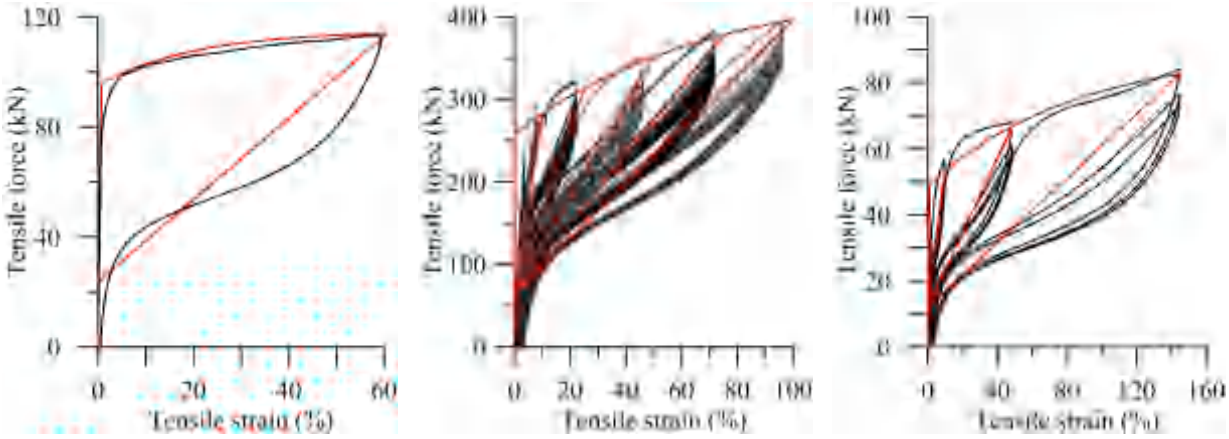

(a) Constantinou *et al.* (2007) (b) Iwabe *et al.* (2000) (c) Warn (2006)

Figure 4. Comparison of experimental and numerical results for LDR bearings in tension (Kumar et al., 2014)

Table 1. Properties of the bearings used for experimental comparison

	Constantinou *et al.* (2007)	Iwabe *et al.* (2000)	Warn (2006)
Diameter, mm	250	500	164
Shape factor, S	9.8	33	10.2
k	60	15	20
a	1.0	1.0	1.0
ϕ_{max}	0.75	0.75	0.75

The behavior of elastomeric bearings under shear and compression is well established. The strength degradation of a LR bearing due to heating of its lead core under cyclic shear loading was validated by Kalpakidis *et al.* (2010). Validation of the coupled horizontal-vertical behavior, and the calculation of buckling load, is presented in Warn *et al.* (2007). Where models had already been validated, the OpenSees user elements were verified by first principles calculations and cross-code comparisons.

The OpenSees user elements ***LeadRubberX*** and ***ElastomericX*** have a similar structure and function, except ***LeadRubberX*** has additional parameters and functions to address heating of the lead core. The ***HDR*** element uses the same mathematical model as ***LeadRubberX*** and ***ElastomericX*** in the axial direction but the model proposed by Grant *et al.* (2004) for shear behavior.

3. Response of base-isolated nuclear power plant

3.1 Numerical model

A two-node macro-model of a nuclear power plant (NPP), shown in Figure 5, is created in OpenSees for response-history analysis. The lumped mass at the top node (node 2) represents the superstructure assigned to one isolator; the superstructure is assumed to be rigid for the purpose

of these analyses. A LR[‡] isolator joins the two nodes: *LeadRubberX*. All six degrees of freedom of the bottom node (node 1) are fixed to the ground, as are the three rotational degrees of freedom at the top node. Although this model cannot capture the effects of rocking and local axial force effects on isolators that are expected in an isolated system, its analysis does allow recommendations to be made about the importance of the five characteristics listed in Section 1.

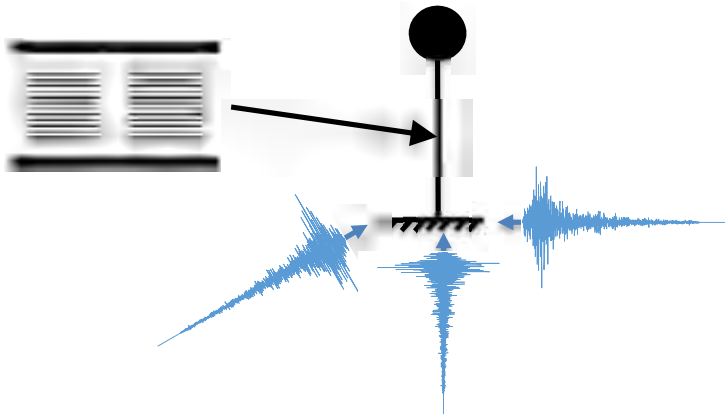

Figure 5. Two-node macro model of a base-isolated NPP

Ten macro-models of base-isolated NPPs are created: two isolation time periods (T = 2, 3 seconds) and five ratios of characteristic strength to supported weight (Q_d / W = 0.03, 0.06, 0.09, 0.12, and 0.15). The models are denoted by $TxQy$, where x identifies the value of T and y identifies the percentage of Q_d / W. Table 2 summarizes the isolator properties assumed for analysis.

Table 2. Geometrical and mechanical properties of elastomeric bearings

Property	Notations (units)	Value
Single rubber layer thickness	t_r (mm)	10
Number of rubber layers	n	31
Total rubber thickness	T_r (mm)	310
Steel shim thickness	t_s (mm)	4.75
Outer diameter	D_o (mm)	1219
Lead core diameter	D_i (mm)	Varies[1]
Cover thickness	t_c (mm)	19
Yield stress of lead	σ_L (MPa)	8.5
Static pressure due to gravity loads	p_{static} (MPa)	3.0
Shear modulus	G (MPa)	Varies[2]

1, 2: Calculated for each model

[‡] Lead-rubber and low damping rubber elastomeric bearings are considered appropriate for use in safety-related nuclear structures in the United States at the time of this writing. Lead-rubber bearings are considered here because the seismic displacements at the Diablo Canyon site were anticipated to be large for design basis shaking.

A static (gravity load) pressure on the bearing of 3 MPa is used for all analyses. The total gravity weight W on the bearing is calculated by multiplying the static pressure by the bonded rubber area. The total weight W is divided by g to obtain the equivalent mass M, which is lumped in the three translational directions at node 2 for response-history analyses. The diameter of the lead core is back calculated from Q_d / W, assuming an initial yield stress of 8.5 MPa. The effective shear modulus is calculated from the isolation time period T of the model. The geometric and mechanical properties of LR bearing are computed from the given values of Q_d / W and T as:

$$W = p_{static} \frac{\pi}{4} D_o^2; A_L = \frac{(Q_d / W) \times W}{\sigma_L}; D_i = \sqrt{4 \frac{A_L}{\pi}}; A = \frac{\pi}{4} \left[\left(D_o + t_c \right)^2 - D_i^2 \right]$$
$$T_r = n t_r; M = \frac{W}{g}; K_{H0} = \frac{4\pi^2 M}{T^2}; G = \frac{K_{H0} T_r}{A} \quad (8)$$

where A_L is the area of the lead core, and all other variables are defined above. The geometric and material properties of the ten LR bearings are summarized in Table 3.

Table 3. Geometric and material properties of LR bearing models

Property	Notations (units)	T2Q3	T2Q6	T2Q9	T2Q12	T2Q15	T3Q3	T3Q6	T3Q9	T3Q12	T3Q15
Lead core diameter	D_i (mm)	125	168	195	216	231	100	136	161	180	195
Shear modulus	G (MPa)	0.92	0.92	0.93	0.94	0.94	0.41	0.41	0.41	0.41	0.41
Horizontal stiffness	K_{H0} (MN/m)	3.52	3.52	3.52	3.52	3.52	1.57	1.57	1.57	1.57	1.57
Vertical stiffness	K_{v0} (MN/m)	4061	4002	3959	3926	3899	3004	2956	2923	2897	2875
Buckling load	P_{cr0} (MN)	67.5	67.3	67.1	67.0	66.9	38.6	38.4	38.3	38.2	38.1
Cavitation force	F_c (MN)	3.28	3.28	3.28	3.28	3.28	1.46	1.46	1.46	1.46	1.46

The parameters of the tensile model, k, a, and $\phi_{\max}$ are set equal to 20, 1.0, and 0.75, respectively, for all models. A sensitivity analyses performed by Kumar *et al.* (2014) showed that the tensile response of an elastomeric bearing is not sensitive to either a or $\phi_{\max}$, and the values a = 1.0 and $\phi_{\max}$ = 0.75 recover the results of experiments. For the large diameter bearings considered here, a very sharp reduction in the tensile stiffness following cavitation is expected, which is captured by k = 20.

The five mechanical behaviors listed in Section 1 are investigated. The ***LeadRubberX*** element permits the user to include each of these behaviors, or a combination thereof, in an analysis through a set of tags. OpenSees does not provide an option for modal damping. Instead, ***Rayleigh*** damping is used, and the multipliers to the mass and stiffness matrices are calculated by assigning 2% damping to the 1st (torsion) and 6th (axial) modes.

The set of 30 three-component recorded ground motions were selected and spectrally matched by Kumar (2015a) to be consistent with uniform hazard response spectra (UHRS) for design-basis earthquake (DBE) shaking at the site of the Diablo Canyon Nuclear Generating Station are used for response-history analysis (Figure 6). The UHRS are calculated for a return period of 10,000 years and 5% damping. The 5% damped horizontal spectral displacements at 2 and 3 seconds are 390 and 510 mm, respectively. The duration of strong motion for the spectrally matched motions ranged between 6.6 and 30.9 seconds. Response-history analysis is performed using these 30 sets of ground motions for each of the ten models at intensities of 100% DBE, 150% DBE, 167% DBE, and 200% DBE shaking. The intensities of 150% DBE and 167% DBE correspond to beyond design basis earthquake in Department of Energy (DOE) and United States Nuclear Regulatory Commission (USNRC) space, respectively; see Huang *et al.* (2009) and Huang *et al.* (2013). The mean 2% damped vertical spectrum is provided to aid later interpretation of the vertical response of the isolation systems.

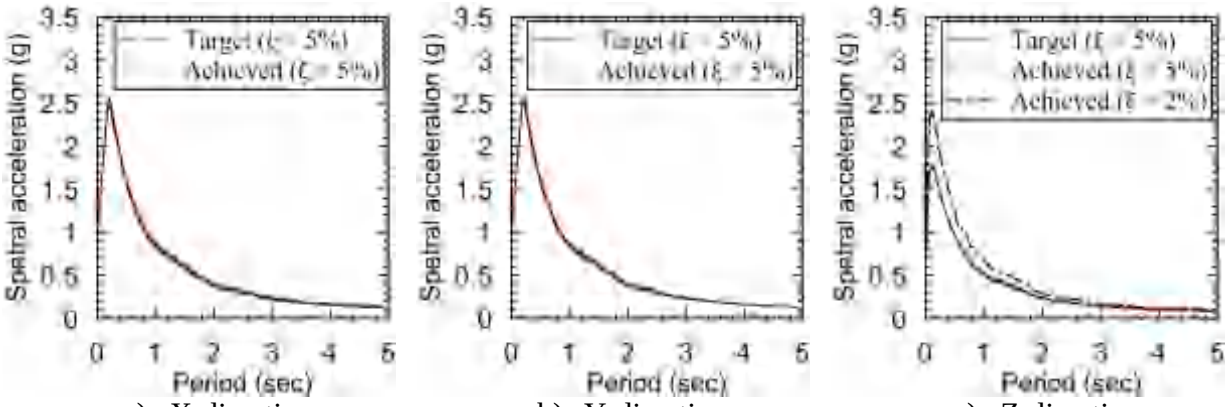

a) X-direction b) Y-direction c) Z-direction

Figure 6. Acceleration response spectra of ground motions (adapted from Kumar (2015a))

The results of the response-history analyses are presented in the following sections. The peak responses for each ground motion set are assumed to distribute lognormally with arithmetic mean μ, median θ, and logarithmic standard deviation σ, which are computed as:

$$\mu = \frac{1}{n}\sum_{i=1}^{n} y_i \qquad \theta = \exp\left(\frac{1}{n}\sum_{i=1}^{n} \ln y_i\right) \qquad \sigma = \sqrt{\frac{1}{n-1}\sum_{i=1}^{n}\left(\ln y_i - \ln\theta\right)^2} \tag{9}$$

where n is the total number of ground motion sets (=30), and y_i is the peak response for *i*th ground motion set. The *p*th percentile (e.g., 50, 90, 99) value, y_p, is calculated as the inverse of the lognormal cumulative distribution function F per Mathworks (2014):

$$y_p = F^{-1}(p \mid \ln\theta, \sigma) = \left\{ y_p : F(y_p \mid \ln\theta, \sigma) = p \right\} \tag{10}$$

These percentiles can be calculated with the aid of normal probability table. MATLAB provides a command *logninv* to compute *p*th percentile values of a lognormal distribution.

3.2 Results of analysis using the simplified isolator model

The simplified model of Figure 1, with equal axial stiffness in compression and tension (and independent of shear displacement), represents the state-of-the-art for response-history analyses of seismically isolated structures using contemporary software programs. The simplified model does not consider any of the five characteristics identified in Section 1. For analysis using the simplified model as implemented in ***LeadRubberX***, all tags are set to 0. The results of the response-history analyses are presented in Table 4 and Table 5.

Mean and 50th, 90th and 99th percentile responses are presented in these tables, noting that the 90th and 99th percentile responses, for beyond design basis and design basis shaking, respectively, are important thresholds for seismically isolated nuclear structures (Huang ***et al.***, 2009; Huang ***et al.***, 2013). Vector sums of the shear displacements and forces are calculated at each time step in an analysis and the peak values for a given ground motion are used to form the distributions of response. The forces are normalized by the total weight W on the bearing, which is approximately equal to 3500 kN for all models.

Table 4. Percentiles of peak horizontal displacement (mm) for 30 ground motion sets; simplified model[1]

	100% DBE					150% DBE				167% DBE				200% DBE			
Model	μ	50^{th}	90^{th}	99^{th}	σ	μ	50^{th}	90^{th}	σ	μ	50^{th}	90^{th}	σ	μ	50^{th}	90^{th}	σ
T2Q3	437	434	500	561	0.11	726	721	837	0.12	828	823	956	0.12	1034	1026	1200	0.12
T2Q6	346	344	400	453	0.12	597	594	686	0.11	688	684	788	0.11	873	867	999	0.11
T2Q9	289	286	346	404	0.15	519	516	600	0.12	602	598	693	0.12	766	761	882	0.11
T2Q12	247	243	307	370	0.18	459	455	544	0.14	538	534	629	0.13	692	687	800	0.12
T2Q15	220	216	276	338	0.19	410	405	496	0.16	483	478	578	0.15	632	626	743	0.13
T3Q3	506	503	573	638	0.10	851	847	963	0.10	979	974	1101	0.10	1240	1235	1382	0.09
T3Q6	381	378	449	517	0.13	684	680	779	0.11	794	790	902	0.10	1012	1006	1147	0.10
T3Q9	321	317	393	469	0.17	572	567	674	0.13	669	664	781	0.13	869	864	994	0.11
T3Q12	283	278	357	438	0.19	506	500	613	0.16	589	582	705	0.15	762	756	898	0.13
T2Q15	261	256	331	409	0.20	459	452	571	0.18	537	530	657	0.17	692	685	833	0.15

1. The horizontal displacement corresponding to 100 (200, 300)% shear strain in the elastomer is 310 (620, 930) mm.

Table 5. Percentiles of peak horizontal shearing force (%W)for 30 ground motion sets; simplified model[1, 2]

	100% DBE					150% DBE				167% DBE				200% DBE			
Model	μ	50^{th}	90^{th}	99^{th}	σ	μ	50^{th}	90^{th}	σ	μ	50^{th}	90^{th}	σ	μ	50^{th}	90^{th}	σ
T2Q3	46	45	52	58	0.11	75	74	86	0.11	85	84	98	0.12	105	105	122	0.12
T2Q6	39	38	44	50	0.11	64	63	73	0.11	73	72	83	0.11	91	90	104	0.11
T2Q9	36	35	41	46	0.12	58	58	66	0.11	66	66	76	0.11	83	82	94	0.11
T2Q12	35	34	40	45	0.12	54	54	63	0.12	62	62	71	0.11	77	77	89	0.11
T2Q15	35	35	40	45	0.11	53	52	61	0.12	59	59	69	0.12	74	73	85	0.11
T3Q3	25	25	28	31	0.09	40	40	45	0.10	45	45	51	0.10	57	57	64	0.09
T3Q6	22	22	25	28	0.10	35	35	39	0.08	40	40	45	0.09	49	49	55	0.09
T3Q9	22	22	25	28	0.11	33	33	37	0.10	37	37	42	0.10	46	46	51	0.09
T3Q12	23	23	26	29	0.09	33	33	37	0.11	36	36	41	0.11	44	44	50	0.10
T2Q15	25	25	28	31	0.09	33	33	38	0.11	37	37	42	0.11	43	43	50	0.11

1. The gravity weight W on the bearing is approximately 3500 kN
2. The characteristic strength, Q_d, ranges between 3%W (e.g., T2Q3) and 15%W (e.g., T3Q15).

3.3 Results of analysis using the advanced isolator model

The advanced isolator model considers the five characteristics of LR bearings identified in Section 1. The effect of each characteristic on the response of the isolated NPP of Section 3.2 is investigated. The responses distribute lognormally (Kumar, 2015b) and the percentiles are calculated from the estimated distribution.

3.3.1 Strength degradation in shear due to heating of the lead core

The percentiles of peak horizontal displacement and force, with and without consideration of heating are presented in Figure 7 and Figure 8, respectively. The responses of models T2Q3 and T3Q3 are not presented because the 90th percentile horizontal displacement at 167% DBE shaking is greater than 1000 mm, and larger diameter lead cores would be used to reduce these displacements. Results for models T2Q15 and T3Q15 are not presented.

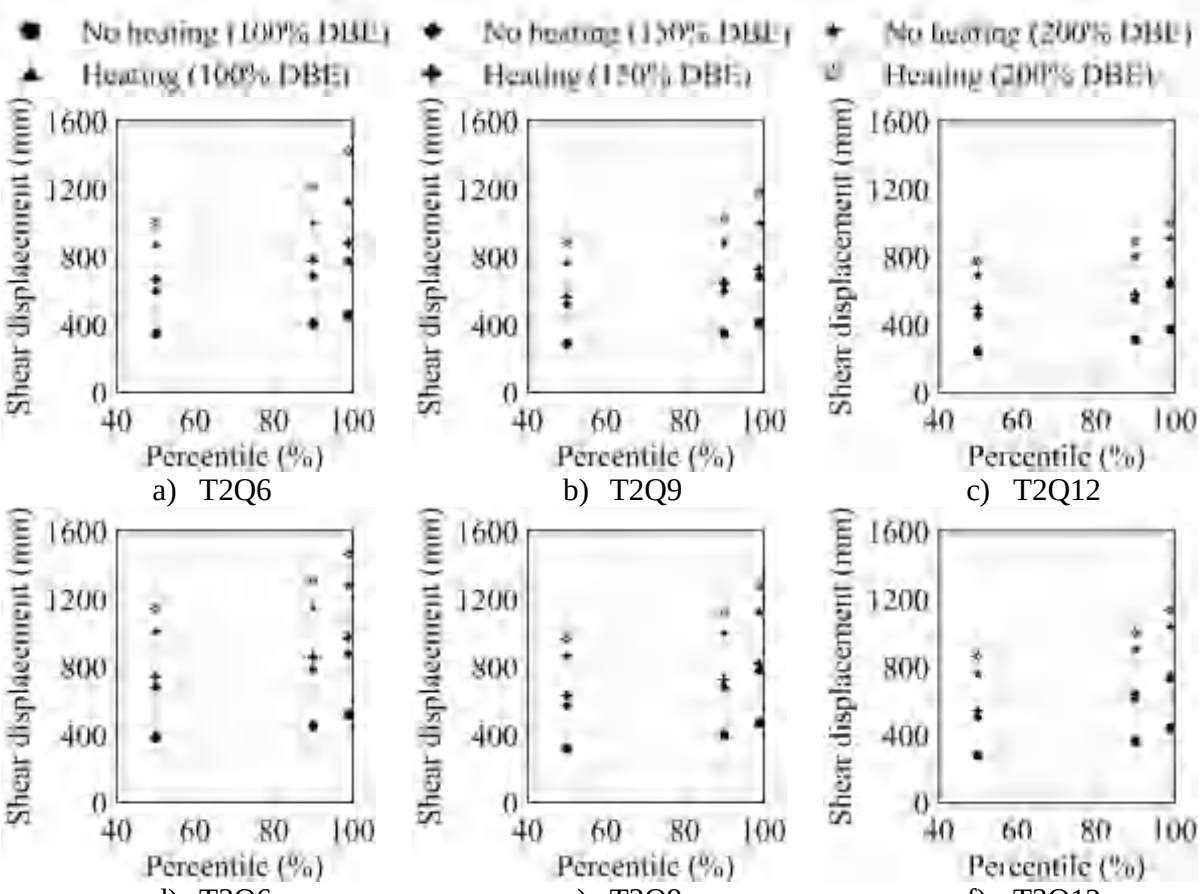

a) T2Q6 b) T2Q9 c) T2Q12

d) T3Q6 e) T3Q9 f) T3Q12

Figure 7. Percentiles of horizontal displacement for LR bearing models

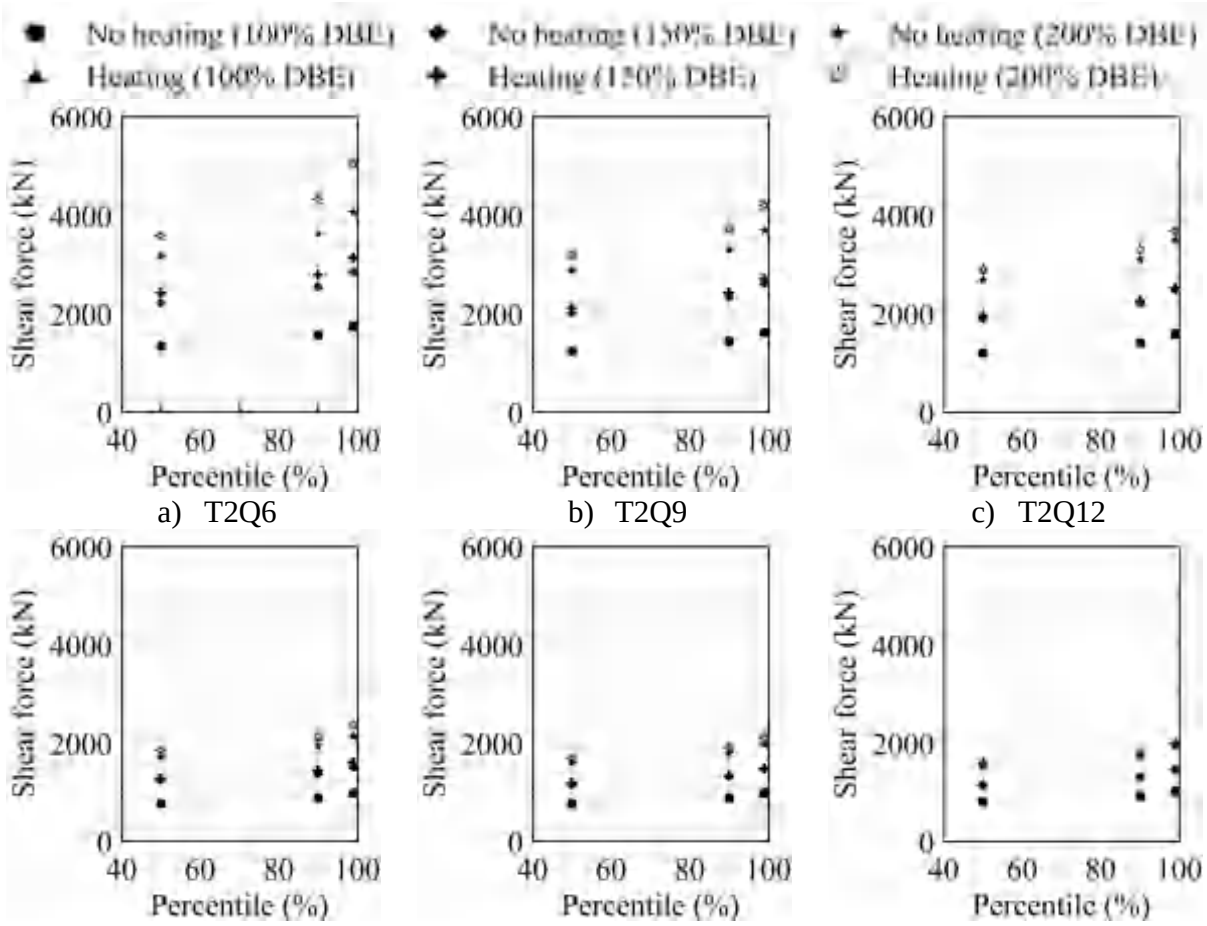

a) T2Q6 b) T2Q9 c) T2Q12

d) T3Q6 e) T3Q9 f) T3Q12

Figure 8. Percentiles of horizontal shear force for LR bearing models

The effect of heating of the lead core on median peak horizontal displacements and shear forces for 100% DBE shaking is negligible at the mean, and 50th, 90th and 99th percentiles. The effect of heating increases with the intensity of earthquake shaking. For the same Q_d / W, the effect of heating decreases with an increase in the isolation period T. For the same period, the effect of heating decreases with increasing Q_d / W. For those isolation systems with the highest Q_d / W (T2Q15 and T3Q15: and not shown above), Kumar (2015b) report that shear force decreases as a result of heating of the lead core.

The characteristic shear strength of a LR bearing varies substantially over the duration of earthquake shaking due to heating of the lead core. Of the ten isolation systems, T2Q6 and T3Q6 show the greatest reduction in characteristic shear strength. Plots of the ratio of the minimum characteristic shear strength to the initial strength, for each ground motion, and three intensities of shaking, are presented in Figure 9. A substantial reduction is observed in the characteristic shear strength with the average minimum value for the thirty ground motions falling below 50% of the initial value at 150% DBE shaking for isolation system T2Q6. Figure 10 plots the maximum temperature rise for each ground motion at three intensities of shaking.

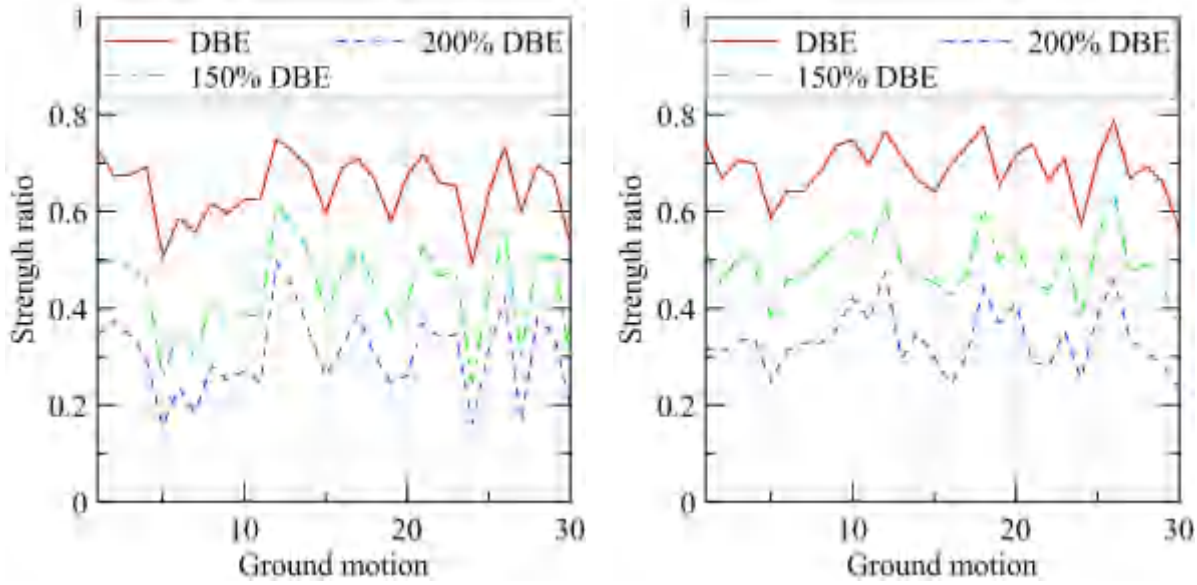

a) T2Q6 b) T3Q6

Figure 9. Ratio of minimum characteristic shear strength to initial strength

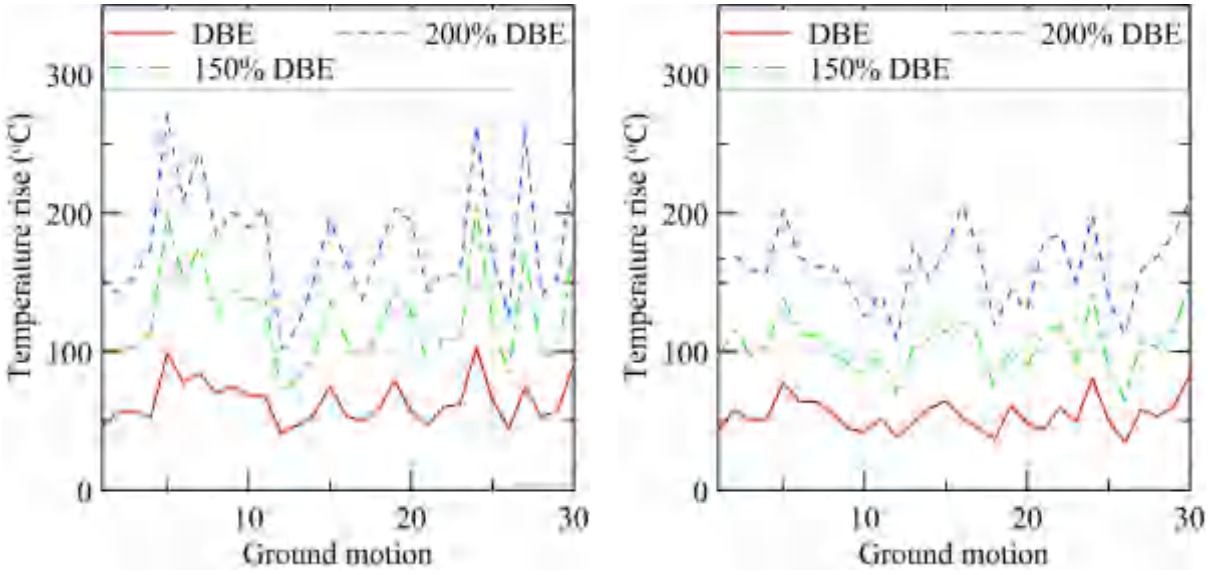

a) T2Q6 b) T3Q6

Figure 10. Maximum temperature rise in the lead core

The maximum change in characteristic strength is observed for ground motions 5 and 30, for isolation systems T2Q6 and T3Q6, respectively. The temperature-rise time series for these two ground motions are presented in Figure 11 noting that the strong motion duration for the horizontal components of ground motions 5 and 30 are 50 seconds.

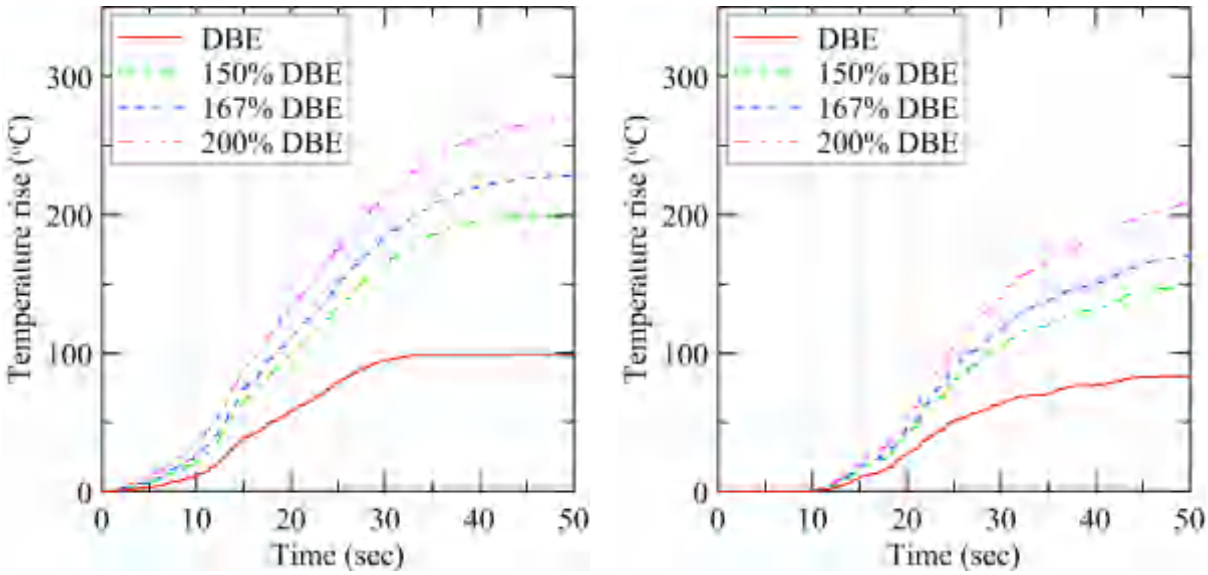

a) T2Q6, ground motion 5 b) T3Q6, ground motion 30

Figure 11. Histories of temperature increase in the lead cores

Rubber has a much lower thermal conductivity and thermal diffusivity than either lead or steel. Accordingly, it can be assumed that heat conducts entirely through the steel shim and end plates of a bearing (Kalpakidis and Constantinou, 2009), with no significant increase in the temperature of the rubber.

3.3.2 Variation in buckling load due to horizontal displacement

The numerical models of elastomeric bearings in contemporary software programs include a linear spring in the vertical direction. Buckling is not modeled. Three models of elastomeric bearings in compression can be modeled in ***LeadRubberX***: 1) linear, 2) bilinear with a constant buckling load P_{cr0}, and 3) bilinear with a buckling load that is dependent on the co-existing horizontal displacement, P_{cr}. These three models are used for response-history analysis to identify the number of ground motions that would trigger buckling at the four intensities of shaking. For the third model, the buckling load calculation suggested by Warn ***et al.*** (2007), and described in Section 2.2.1, is used.

Plots of the axial load ratio, which is the ratio of the minimum critical buckling load of a bearing over the duration of a ground motion, $P_{cr\min}$, as predicted by (4) to the buckling load at zero displacement, P_{cr0}, are presented in Figure 12. The buckling load varies substantially over the duration of some of the earthquake ground motions. A bearing will never achieve its critical buckling load at zero horizontal displacement under three components of input as it will fail at a lower axial load at a nonzero horizontal displacement. For the constant buckling load model, the ratio is 1.0 for the duration of a ground motion. The use of a buckling load calculated at zero horizontal displacement might provide misleading expectations of the performance of isolators and an isolation system in design basis and more intense earthquake shaking.

The ratio of the instantaneous axial load to the instantaneous buckling load is computed at each time step in each response-history analysis, and the maximum value is recorded. If the ratio exceeds unity, the isolator has buckled. Plots of the maximum value of the ratio for each ground motion, at three intensities of shaking, are presented in Figure 13 and Figure 14 for the constant and displacement-dependent buckling load models, respectively, for T2Q6 and T3Q6. Other data are presented in Kumar (2015b).

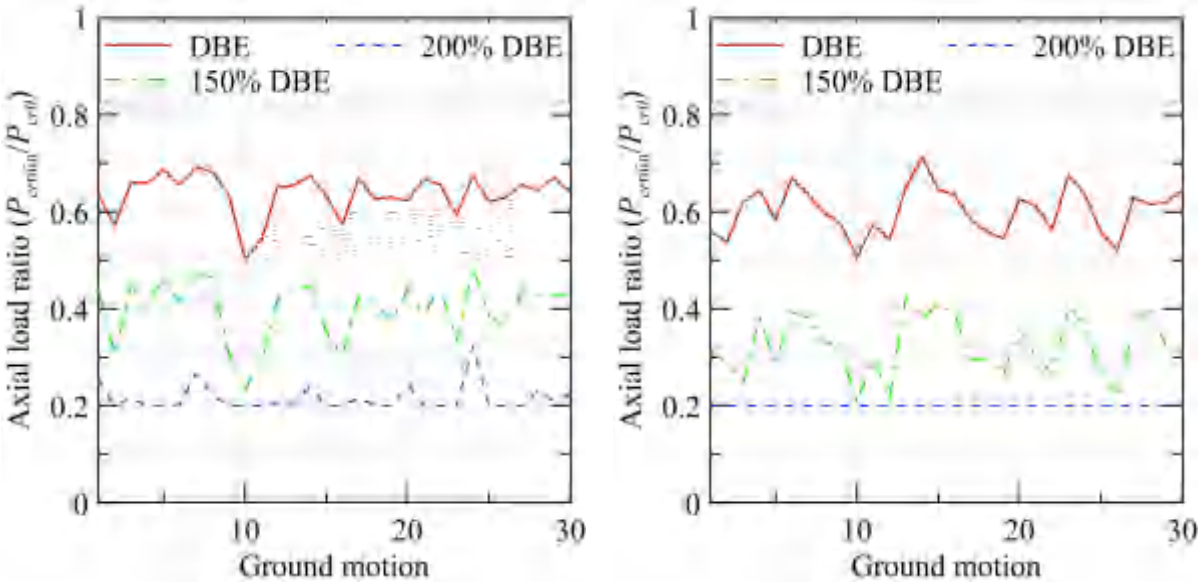

a) T2Q6 b) T3Q6

Figure 12. Normalized axial load ratios

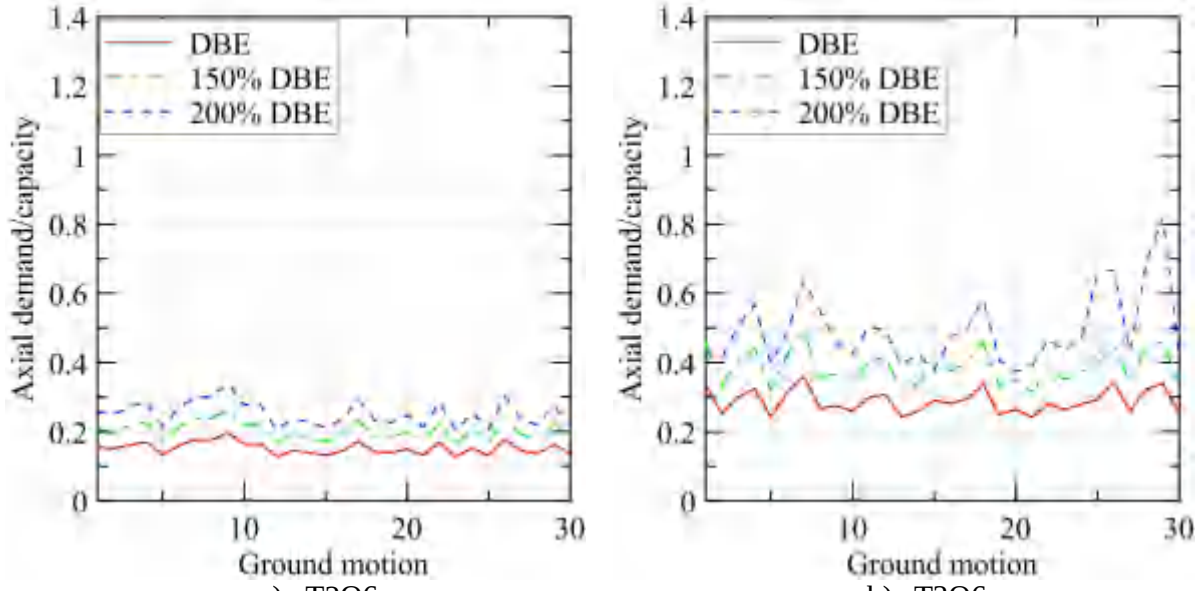

a) T2Q6 b) T3Q6

Figure 13. Demand/capacity ratios for the constant buckling load model, P_{cr0}

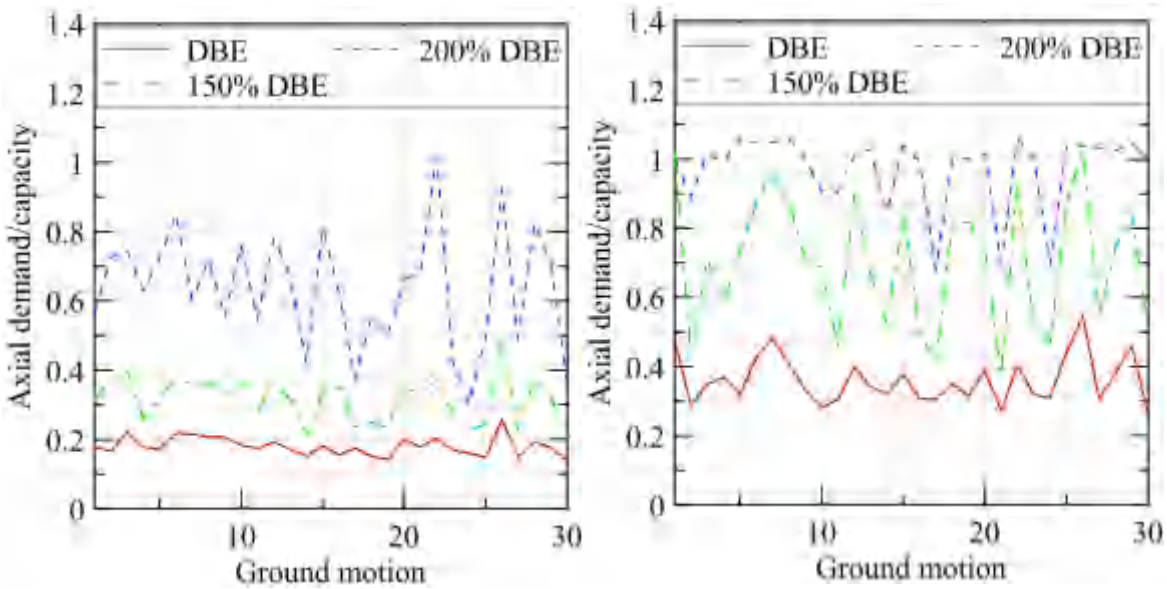

a) T2Q6 b) T3Q6

Figure 14. Demand/capacity ratios for the displacement-dependent buckling load model, P_{cr}

The numbers of ground motions for which buckling is predicted using the constant and the displacement-dependent buckling load models are summarized in Table 6, for T2Q6 and T3Q6. Model T2Q6 has a greater margin against buckling (i.e., smaller demand-to-capacity ratio) than T3Q6. The use of a buckling load calculated at zero displacement (i.e., P_{cr0}) may lead to substantially non-conservative judgments regarding performance of isolation systems, noting however that buckling of individual isolators in extreme shaking may not compromise the performance of an isolation system composed of 100s of isolators.

Table 6. Number of ground motions (of 30) triggering buckling failures

Intensity (% DBE)	T2Q6		T3Q6	
	Using P_{cr0}	Using P_{cr}	Using P_{cr0}	Using P_{cr}
100	0	0	0	0
150	0	0	0	2
167	0	0	0	12
200	0	1	0	20

3.3.3 Cavitation and post-cavitation behavior due to tensile loading

A nonlinear elastic model is used to capture the behavior of elastomeric bearings in cyclic tension. The number of ground motions that produce cavitation damage at each intensity level

are identified in Table 7. Nearly 50% of the ground motions result in cavitation at 100% DBE shaking for the 2 sec isolation systems, and all or nearly all of the ground motions result in cavitation at 150% DBE shaking for the 2 and 3 sec isolation systems. These high fractions are due to the intense vertical shaking at the Diablo Canyon site. The period of vibration in the axial direction for the 2 and 3 sec isolation systems are 0.06 and 0.07 sec, respectively, and the 2% damped vertical spectral acceleration at these periods exceed 2.2g at 100% DBE shaking (see Figure 6c).

Table 7. Number of ground motions (of 30) that cavitate isolators

Intensity	Isolation system									
(% DBE)	T2Q3	T2Q6	T2Q9	T2Q12	T2Q15	T3Q3	T3Q6	T3Q9	T3Q12	T3Q15
100	12	14	14	16	16	27	27	27	27	27
150	27	27	27	27	28	30	30	30	30	30
167	28	28	28	28	28	30	30	30	30	30
200	30	30	30	29	29	30	30	30	30	30

3.3.4 Variation in axial stiffness due to horizontal displacement

The horizontal and vertical responses of an elastomeric bearing are coupled through the axial stiffness that in turn depends on the co-existing horizontal displacement. The elastic shear stiffness of a LR bearing is given by (2). Axial stiffness (and buckling load) decreases with increasing horizontal displacement. Figure 15 shows the response of a LR bearing (LR5 in Warn (2006)) subject to a vertical acceleration history (in m^2/s) of $2.6\sin(20\pi t)$ in the vertical direction. Two models for axial stiffness are considered here: 1) axial stiffness per (2), and 2) axial stiffness per Figure 3, which is (2) but capped by buckling and cavitation. Results are presented in Figure 15a and Figure 15b, respectively, for the three values of horizontal displacement, normalized by the outer diameter of the bearing, D_o, equal to 152 mm.

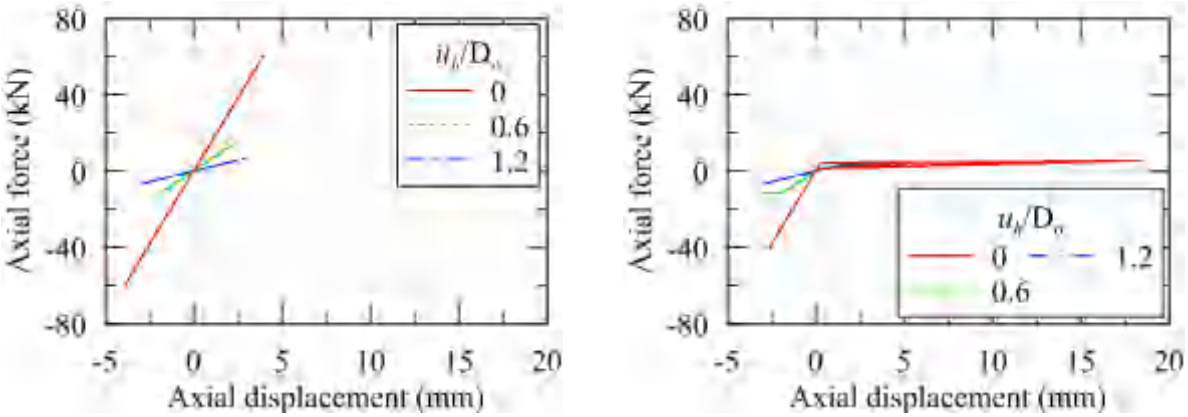

a) Axial stiffness variation per Eqn. (2)

b) Axial stiffness + buckling + cavitation per Figure 3

Figure 15. Axial response of bearing LR5 in Warn (2006) subject to harmonic vertical excitation

The axial response of this bearing is substantially impacted by considerations of co-existing horizontal displacement, noting that the simplified model would predict response given by the red ($u_h / D_o = 0$) line in Figure 15a.

To understand the influence of co-existing horizontal displacement on the vertical response of an isolation system, analyses are performed for two representations of axial stiffness: 1) equal stiffness in compression and tension, calculated at zero horizontal displacement: K_{v0} in (2), and 2) equal axial stiffness in compression and tension, but varying as a function of horizontal displacement: K_v in (2). Cavitation and buckling are not considered. Results for a sample isolation system, T3Q6, are presented in Figure 16. Results for the remaining isolation systems will be available in Kumar (2015b). The influence is negligible for 100% DBE shaking but considerable for beyond design basis shaking, with changes in axial displacement being greater than those in axial force.

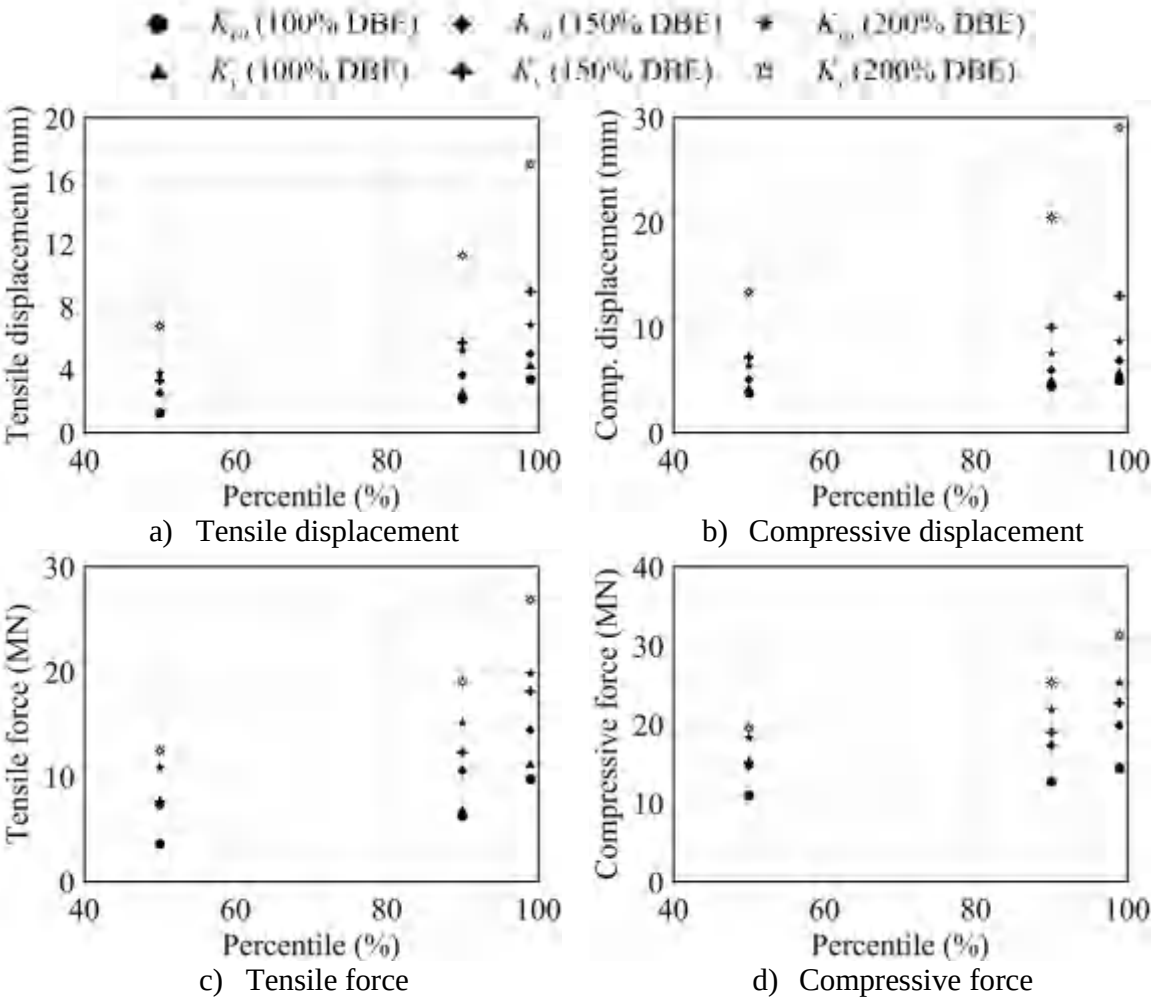

a) Tensile displacement b) Compressive displacement

c) Tensile force d) Compressive force

Figure 16. Influence of axial stiffness model on the vertical response of T3Q6

The variation in the stiffness ratio, which is the ratio of the minimum axial stiffness over the duration of a ground motion to the axial compressive stiffness at zero displacement, is shown in Figure 17a, and the history of the ratio of the instantaneous axial compressive stiffness to the initial axial compressive stiffness for T3Q6 and ground motion 30 is shown in Figure 17b. The minimum axial compressive stiffness drops below 40% of the initial stiffness at 150+% DBE shaking. Although the variation in axial compressive stiffness has a notable effect on axial response, its effect on horizontal response is negligible here because the axial force varies at a much higher frequency than the isolation-system response in the horizontal direction[§].

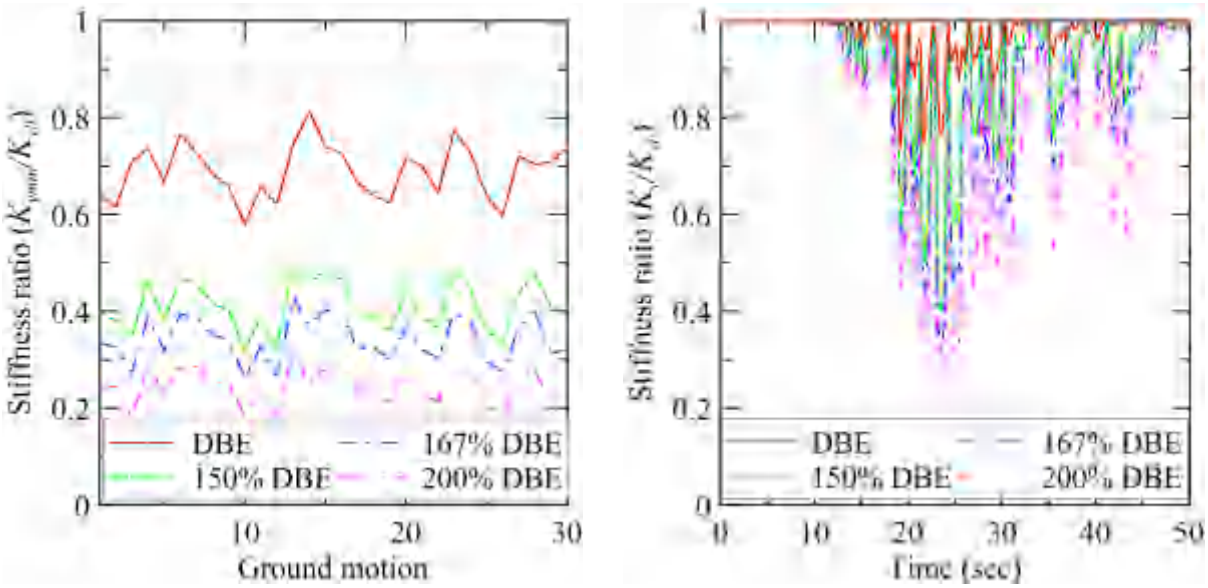

a) Minimum axial stiffness b) Instantaneous axial stiffness for GM30

Figure 17. Effect of the variation of axial compressive stiffness

3.3.5 Variation in shear stiffness due to axial load

The shear stiffness of an elastomeric bearing depends on the instantaneous axial load per (3). Two values for the buckling load can be used in (3): 1) buckling load at zero lateral displacement, P_{cr0}, and 2) buckling load, P_{cr}, per Eqn. (4). Three models of the LR bearing are used to investigate the choice of shear stiffness model: 1) shear stiffness independent of axial load, 2) axial load dependence of shear stiffness using $P_{cr} = P_{cr0}$, and 3) axial load dependence of shear stiffness using the instantaneous buckling load, P_{cr}.

Figure 18a and Figure 18b present the results of response-history analysis of model T2Q6 using one ground motion from the set of 30, scaled to 167% DBE shaking. Models 1, 2, and 3 in the legend are: 1) Shear stiffness K_{H0} independent of axial load, 2) shear stiffness K_H dependent on axial load using P_{cr0} for the buckling load in (3), and 3) shear stiffness K_H dependent on axial load using P_{cr} for the buckling load in (3). The peak horizontal displacement is not affected by

[§] The effect of changing axial compressive stiffness on shear response may be important if rocking-induced axial forces are significant because the rocking frequency may be of the order of the isolation-system frequency.

the choice of the model. The fluctuations in the hysteresis loops of models 2 and 3 occur at time instants near peak displacement, but do not increase the shearing forces transmitted to the superstructure. Figure 18b presents fluctuations in the shear stiffness, calculated as the shear stiffness of models 2 and 3 normalized by the shear stiffness of model 1, which is 3.52 MN/m.

The outcomes of the response-history analysis of the ten base-isolated NPP models for the other ground motion sets, at all four intensities of shaking, are virtually identical to those seen in Figure 18, namely, that ignoring the effect of axial load on horizontal stiffness does not compromise the calculation of peak horizontal displacements, or transmitted shear force to the superstructure.

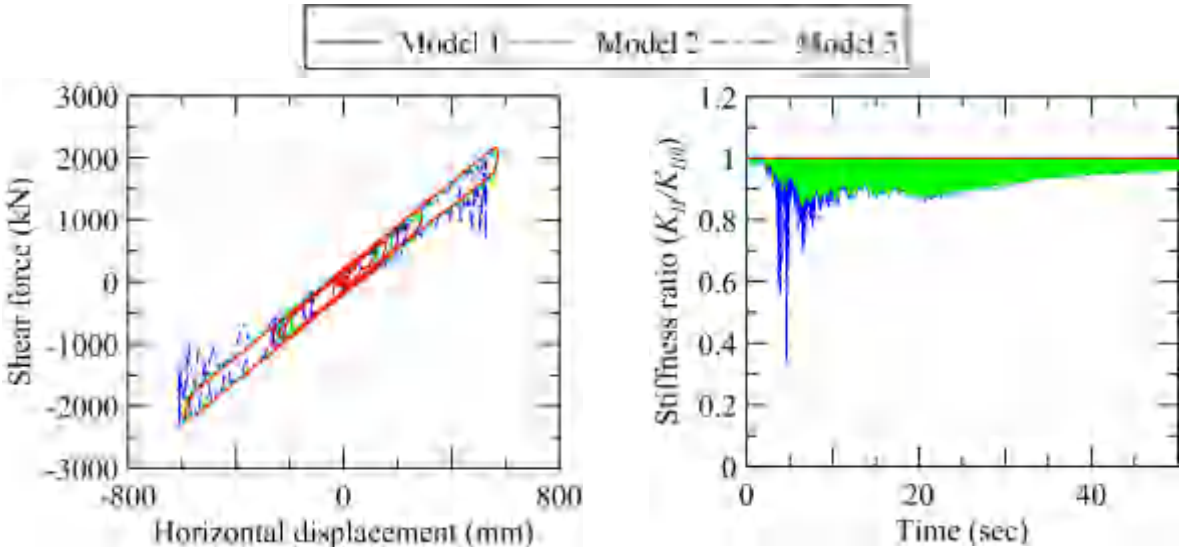

a) Shear response b) Variation in normalized shear stiffness

Figure 18. Response of T2Q6 to ground motion 1 at 167% DBE

3.3.6 Cumulative effects

The responses of the ten models considering all five characteristics listed in Section 1 are considered next.

The ratios of the percentiles of the peak shear displacement for the simplified and advanced base-isolated NPP models, considered separately, at different intensities of shaking, are presented in Figure 19, where D is the displacement and its subscript denotes the intensity and the percentile of the peak shear displacement. Figure 20 presents horizontal displacements obtained using the advanced models normalized by the median DBE horizontal displacement calculated using the simplified model. The plots in the figures can be used to estimate horizontal displacements at 150+% DBE shaking for a range of isolation systems by calculating the median DBE horizontal displacement. For example, the DBE median horizontal displacement obtained using a simplified model can be increased by the ratios presented in Figure 20 to address the five intra-earthquake changes in the mechanical properties of LR bearings enumerated in Section 1.

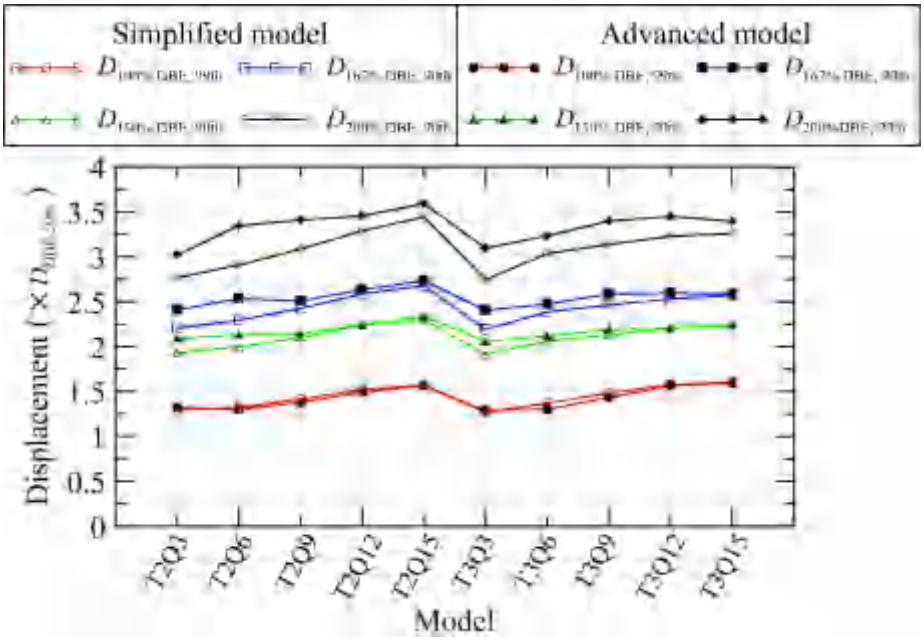

Figure 19. Ratios of percentiles of peak horizontal displacement to the median DBE displacement; simplified and advanced models

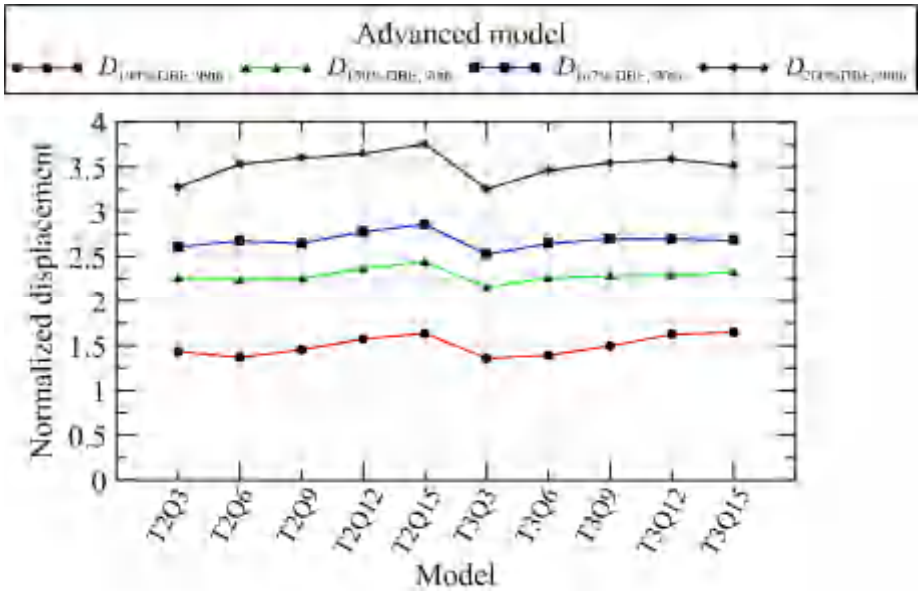

Figure 20. Ratios of the percentiles of peak horizontal displacement calculated using the advanced model to the median DBE displacement calculated using the simplified model

The numbers of ground motions for which cavitation and buckling are predicted are identified in Table 8 and Table 9, respectively, noting that simplified model of Section 3.2 cannot account for either behavior. The use of a displacement-dependent model for calculation of buckling load predicts instabilities in many cases for the intensities greater than DBE. Flexible (longer period) isolation systems with low strength (e.g., T3Q3) are more vulnerable to buckling. The results of response-history analyses for which buckling is predicted are not included in the calculation of the percentiles presented in Table 10 through Table 12. Only mean values are reported in shaded cells for these shaking intensities at which 15 or more (of 30) ground motions result in isolator buckling.

Peak horizontal displacements are summarized in Table 10. The 90th percentile horizontal strain in the LR bearings at 167% DBE shaking is smaller than 300% for all isolation systems except those with low strength (e.g., T2Q3). The peak shearing and compressive forces normalized by the gravity load W are presented in Table 11 and Table 12, respectively. Stiff (shorter period) isolation system transmits greater shear forces to the superstructure, with the mean values for T2Q3 and T2Q6 exceeding 100%W at 200% DBE shaking. For the normalized compressive forces in Table 12, the increment above 100 represents the effect of the vertical ground motion. The high intensity of the vertical shaking at the site of the Diablo Canyon Nuclear Generating Station is reflected in these compressive forces, with mean values at 200% DBE above 600%W for all models. This value is greater than that calculated by summing gravity and earthquake forces calculated using the peak spectral ordinate of the 2% damped vertical spectrum of Figure 6c ($5.4W = W + 2*2.2W$) because the vertical damping ratio falls below 2%. (The Rayleigh damping coefficients were selected by assigning 2% damping to the vertical frequency calculated using axial stiffness at zero horizontal displacement: the decrease in the vertical frequency due to a reduction in axial stiffness associated with horizontal displacement results in a smaller damping ratio than 2%.)

Peak tensile forces normalized by the initial cavitation force, F_c, are presented in Table 13. Mean values are reported because the data did not fit a lognormal distribution. The mean peak tensile forces exceed the cavitation force at 150%DBE shaking due to the intense vertical shaking at the Diablo Canyon site.

Table 8. Number of ground motion sets (of 30) for which cavitation is predicted; advanced model

Intensity (% DBE)	Isolation system									
	T2Q3	T2Q6	T2Q9	T2Q12	T2Q15	T3Q3	T3Q6	T3Q9	T3Q12	T3Q15
100	15	15	15	16	14	29	28	29	29	29
150	29	29	28	28	28	30	30	30	30	30
167	29	29	29	28	28	30	30	30	30	30
200	30	30	30	30	30	30	30	30	30	30

Table 9. Number of ground motion sets (of 30) for which buckling is predicted; advanced model

Intensity (% DBE)	Isolation system									
	T2Q3	T2Q6	T2Q9	T2Q12	T2Q15	T3Q3	T3Q6	T3Q9	T3Q12	T3Q15
100	0	0	0	0	0	0	0	0	0	0
150	0	0	0	0	0	15	7	2	1	0
167	3	0	0	0	0	24	19	10	8	8
200	12	8	2	2	0	29	27	22	24	19

Table 10. Percentiles of peak horizontal displacement (mm) for 30 ground motion sets; advanced model

	100% DBE					150% DBE				167% DBE				200% DBE			
Model	μ	50th	90th	99th	σ	μ	50th	90th	σ	μ	50th	90th	σ	μ	50th	90th	σ
T2Q3	473	470	548	621	0.12	816	807	977	0.15	946	934	1148	0.16	1209	--	--	--
T2Q6	365	363	419	470	0.11	669	664	774	0.12	784	777	918	0.13	1040	1029	1246	0.15
T2Q9	305	302	360	415	0.14	563	559	646	0.11	663	659	758	0.11	889	881	1040	0.13
T2Q12	261	257	320	383	0.17	497	493	575	0.12	587	583	675	0.11	773	768	894	0.12
T2Q15	229	225	288	353	0.19	444	440	526	0.14	527	523	617	0.13	702	697	810	0.12
T3Q3	535	533	608	676	0.10	978	--	--	--	1209	--	--	--	1584	--	--	--
T3Q6	407	405	467	524	0.11	734	731	828	0.10	847	--	--	--	1148	--	--	--
T3Q9	335	331	404	474	0.15	633	629	732	0.12	728	--	--	--	927	--	--	--
T3Q12	295	290	371	453	0.19	541	536	638	0.14	641	636	749	0.13	850	--	--	--
T3Q15	271	265	343	422	0.20	490	483	598	0.17	581	574	705	0.16	726	--	--	--

1. The horizontal displacement corresponding to 100 (200, 300)% shear strain in the elastomer is 310 (620, 930) mm.
2. Shaded cell data correspond to the cases where buckling is predicted in more than 15 ground motion sets; only mean values are reported.

Table 11. Percentiles of peak shearing force; advanced model (%W)for thirty ground motion sets; advanced model

	100% DBE					150% DBE				167% DBE				200% DBE			
Model	μ	50th	90th	99th	σ	μ	50th	90th	σ	μ	50th	90th	σ	μ	50th	90th	σ
T2Q3	48	48	56	63	0.11	80	79	94	0.13	91	91	109	0.15	116	--	--	--
T2Q6	40	39	45	50	0.11	68	68	78	0.11	79	78	90	0.11	102	101	120	0.13
T2Q9	36	36	41	46	0.11	60	60	68	0.10	70	69	79	0.10	90	89	103	0.11
T2Q12	34	34	40	45	0.12	56	55	64	0.11	64	64	73	0.11	81	81	93	0.11
T2Q15	34	34	40	45	0.12	53	53	61	0.11	60	60	69	0.11	76	76	87	0.11
T3Q3	25	25	28	31	0.09	40	--	--	--	46	--	--	--	58	--	--	--
T3Q6	22	22	25	27	0.09	35	35	38	0.08	37	--	--	--	48	--	--	--
T3Q9	22	21	25	28	0.11	34	33	38	0.10	37	--	--	--	42	--	--	--
T3Q12	22	22	26	29	0.11	32	32	37	0.11	36	36	41	0.11	41	--	--	--
T3Q15	24	24	27	30	0.10	32	32	37	0.11	36	36	42	0.12	41	--	--	--

1. The gravity weight W on the bearing is approximately 3500 kN.
2. The characteristic strength, Q_d, ranges between 3%W (e.g., T2Q3) to 15%W (e.g., T3Q15).
3. Shaded cell data correspond to the cases where buckling is predicted in more than 15 ground motion sets; only mean values are reported.

Table 12. Percentiles of peak compressive force (% W) for 30 ground motion sets; advanced model

	100% DBE					150% DBE				167% DBE				200% DBE			
Model	μ	50th	90th	99th	σ	μ	50th	90th	σ	μ	50th	90th	σ	μ	50th	90th	σ
T2Q3	306	304	362	417	0.14	455	445	586	0.22	550	523	777	0.31	637	--	--	--
T2Q6	305	301	361	419	0.14	457	441	618	0.26	546	530	737	0.26	629	607	865	0.28
T2Q9	303	299	360	418	0.14	467	437	667	0.33	522	503	723	0.28	649	626	899	0.28
T2Q12	303	300	365	428	0.15	461	442	633	0.28	565	529	823	0.34	647	618	909	0.30
T2Q15	302	299	361	421	0.15	474	445	674	0.32	539	515	754	0.30	691	651	1021	0.35
T3Q3	354	343	464	594	0.24	517	--	--	--	571	--	--	--	752	--	--	--
T3Q6	343	333	443	560	0.22	503	485	688	0.27	569	--	--	--	517	--	--	--
T3Q9	343	334	445	563	0.22	565	543	787	0.29	557	--	--	--	590	--	--	--
T3Q12	330	326	402	477	0.16	561	542	762	0.26	563	552	721	0.21	558	--	--	--
T3Q15	338	331	426	522	0.20	529	515	690	0.23	570	554	755	0.24	669	--	--	--

1. The gravity weight W on the bearing is approximately 3500 kN
2. Shaded cell data correspond to the cases where buckling is predicted in more than 15 ground motion sets; only mean values are reported.

Table 13. Mean peak tensile force (% F_c); of 30 ground motion sets; advanced model

	100% DBE	150% DBE	167% DBE	200% DBE
Model	μ	μ	μ	μ
T2Q3	87	100	102	104
T2Q6	84	99	101	103
T2Q9	84	99	101	103
T2Q12	81	98	101	104
T2Q15	81	99	101	103
T3Q3	98	103	104	105
T3Q6	98	103	104	103
T3Q9	98	103	104	105
T3Q12	98	103	103	104
T3Q15	99	103	104	105

1. The cavitation force F_c corresponds to 3276 kN and 1456 kN for 2 and 3 sec isolation period models, respectively

4. Summary and conclusions

Mathematical models of LDR and LR bearings that can be used for analysis of base-isolated nuclear structures under design and beyond design basis shaking are presented. These mathematical models extend the available robust formulation in shear and compression, and a new phenomenological model is implemented for behavior under tension. The phenomenological model uses three unknown parameters that are determined by experiments.

Ten models of a base-isolated NPP are analyzed using thirty sets of ground motions that are selected and scaled to be consistent with uniform hazard response spectra for a return period of 10,000 years (or DBE shaking) at the site of the Diablo Canyon Nuclear Generating Station. A two-node macro-model is used for response- history analysis, noting that such a model cannot account for the effects of rocking and torsion. Two types of LR bearing models are analyzed. The first is the simplified model that is widely used and implemented in contemporary software programs, whereas the second is an advanced model that addresses five mechanical characteristics of elastomeric bearings under extreme loading:

1. Strength degradation in shear due to heating of the lead core (LR bearings only)
2. Variation in buckling load due to horizontal displacement
3. Cavitation and post-cavitation behavior due to tensile loading
4. Variation in axial stiffness due to horizontal displacement
5. Variation in shear stiffness due to axial load

The advanced model, which was verified and validated per ASME best practices, is implemented as user element ***LeadRubberX*** in OpenSees. The influence of each characteristic and of the combination of the five characteristics, are investigated, and results are compared with those obtained using the simplified model. The main conclusions of the study, which are specific to a region of moderate to high seismic hazard, are:

1. Heating of the lead core has a relatively small effect (< 10%) on horizontal DBE shear displacements but the influence increases at higher intensities of shaking.
2. Peak horizontal displacement is more sensitive to the heating of lead cores than peak shear force.
3. For a given isolation period, the effect of lead core heating decreases with an increase in the ratio of characteristic strength to weight, whereas for a given value of the ratio, the effect decreases with an increase in isolation period.
4. The characteristic strength of a LR bearing may degrade substantially during extreme earthquake shaking, with values falling below half the initial value for 150+% DBE shaking.
5. The temperature in a lead core may rise by 100+ °C for 150+% DBE shaking.
6. The axial response of a NPP base-isolated with LR bearings is not affected by changes in the mechanical properties of the lead core due to heating.
7. The buckling load of a LR bearing varies substantially during earthquake shaking. The displacement-dependent model for buckling load predicts failure for many more ground motions than the constant buckling load model, and is recommended for use in practice.

8. No effect of the variation in axial compression stiffness with lateral displacement is observed on the axial response at DBE shaking. A moderate effect is observed at higher intensities of shaking.
9. The horizontal (shear) force response of a base-isolated NPP is not affected by variations in axial compressive stiffness due to lateral displacements.
10. Of the five characteristics of LR bearings discussed in Section 1, 1) strength degradation due to heating of the lead core, 2) variation in buckling load due to horizontal displacement, and 3) variation in axial stiffness due to horizontal displacement affect the responses of a base-isolated NPP most significantly.

ACKNOWLEDGEMENTS

This research project is supported by a grant to MCEER from the United States Nuclear Regulatory Commission (USNRC) and the Lawrence Berkeley National Laboratory (LBNL). This financial support is gratefully acknowledged. The authors thank Dr. Annie Kammerer, formerly of the USNRC, for providing the site-specific hazard data for the site of the Diablo Canyon Nuclear Generating Station, Dr. Robert Budnitz of LBNL for effectively managing the project and advising the authors on the issues related to the analysis and design of the nuclear structures, and former University at Buffalo graduate student Dr. Gordon Warn of Penn State University for providing test data on elastomeric bearings.

REFERENCES

American Society of Mechanical Engineers (ASME). (2006). "Guide for verification and validation in computational solid mechanics." *ASME V&V 10–2006*, New York, NY.

Buckle, I. G., and Liu, H. (1993). "Stability of elastomeric seismic isolation systems." *Proceedings: 1st Seminar on Seismic Isolation, Passive Energy Dissipation, and Control*, Redwood City, CA, 293-305.

Constantinou, M. C., Whittaker, A. S., Kalpakidis, Y., Fenz, D. M., and Warn, G. P. (2007). "Performance of seismic isolation hardware under service and seismic loading." Report MCEER-07-0012, Multidisciplinary Center for Earthquake Engineering Research, State University of New York at Buffalo, NY.

Grant, D. N., Fenves, G. L., and Whittaker, A. S. (2004). "Bidirectional modeling of high-damping rubber bearings." *Journal of Earthquake Engineering*, 8(Supplement 001), 161-185.

Huang, Y.-N., Whittaker, A. S., Kennedy, R. P., and Mayes, R. L. (2009). "Assessment of base-isolated nuclear structures for design and beyond-design basis earthquake shaking." Report MCEER-09-0008, Multidisciplinary Center For Earthquake Engineering Research, State University of New York at Buffalo, NY.

Huang, Y.-N., Whittaker, A. S., Kennedy, R. P., and Mayes, R. L. (2013). "Response of base-isolated nuclear structures for design and beyond-design basis earthquake shaking." *Earthquake Engineering & Structural Dynamics*, 42(3), 339–356.

Iwabe, N., Takayama, M., Kani, N., and Wada, A. (2000). "Experimental study on the effect of tension for rubber bearings." *Proceedings: 12th World Conference on Earthquake Engineering*, New Zealand.

Kalpakidis, I. V., Constantinou, M. C., and Whittaker, A. S. (2010). "Modeling strength degradation in lead-rubber bearings under earthquake shaking." *Earthquake Engineering and Structural Dynamics*, 39(13), 1533-1549.

Koh, C. G., and Kelly, J. M. (1987). "Effects of axial load on elastomeric isolation bearings." Report EERC/UBC-86/12, Earthquake Engineering Research Center, University of California, Berkeley, CA.

Kumar, M. (2014). Computer Program ElastomericX, LeadRubberX, and HDR: User elements in OpenSees for analysis of elastomeric seismic isolation bearings under extreme loading, OpenSees, Buffalo, NY, (http://opensees.berkeley.edu/wiki/index.php).

Kumar, M., Whittaker, A., and Constantinou, M. (2014). "An advanced numerical model of elastomeric seismic isolation bearings." *Earthquake Engineering & Structural Dynamics*, 43(13), 1955-1974.

Kumar, M. (2015a). "Seismic isolation of nuclear power plants using sliding bearings." Ph.D. Dissertation, University at Buffalo, The State University of New York, Buffalo, NY.

Kumar, M. (2015b). "Seismic isolation of nuclear power plants using elastomeric bearings." Ph.D. Dissertation, University at Buffalo, The State University of New York, Buffalo, NY.

The Mathworks Inc. (Mathworks) (2014). Computer Program Matlab R2014a, Natick, MA.

McKenna, F., Fenves, G., and Scott, M. (2006). Computer Program OpenSees: Open system for earthquake engineering simulation, Pacific Earthquake Engineering Center, University of California, Berkeley, CA., (http://opensees.berkeley.edu).

Nagarajaiah, S., Reinhorn, A. M., and Constantinou, M. C. (1991). "Nonlinear dynamic analysis of 3-d-base-isolated structures." *Journal of Structural Engineering*, 117(7), 2035-2054.

Park, Y. J., Wen, Y. K., and Ang, A. H. S. (1986). "Random vibration of hysteretic systems under bi-directional ground motions." *Earthquake Engineering & Structural Dynamics*, 14(4), 543-557.

Ryan, K. L., Kelly, J. M., and Chopra, A. K. (2005). "Nonlinear model for lead-rubber bearings including axial-load effects." *Journal of Engineering Mechanics*, 131(12), 1270-1278.

Warn, G. P. (2006). "The coupled horizontal-vertical response of elastomeric and lead-rubber seismic isolation bearings." Ph.D. Dissertation, The State University of New York at Buffalo, Buffalo, NY.

Warn, G. P., Whittaker, A. S., and Constantinou, M. C. (2007). "Vertical stiffness of elastomeric and lead-rubber seismic isolation bearings." *Journal of Structural Engineering*, 133(9), 1227-1236.

Wen, Y.-K. (1976). "Method for random vibration of hysteretic systems." *Journal of the Engineering Mechanics Division*, 102(2), 249-263.